Effects of air movement in a hot air dryer on the drying characteristics of colored potato (*Solanum tuberosum* L.) using computational fluid dynamics

Hyeon Woo Park, Won Byong Yoon*

(*Department of Food Science and Biotechnology, College of Agriculture and Life Science, Kangwon National University, Chuncheon, Gangwon 200-701, S. Korea*)

Abstract: The flow fields of hot air in the dryer for drying colored potatoes of which characteristics are highly sensitive to the temperature were simulated using computational fluid dynamics (CFD) simulation. The local air velocity decreased as the distance from the flow inlet increased. The mass and heat transfer coefficients increased from 0.666×10^{-2} m/s to 1.711×10^{-2} m/s, and 6.555 W/(m^2·K) to 16.834 W/(m^2·K), respectively, as the air velocity increased from 0.207 m/s to 1.567 m/s at 60°C. The drying simulation model using the heat and mass transfer model made accurate predictions. The thermal properties of colored potato, such as the thermal conductivity and specific heat, decreased significantly from 0.440 W/(m·K) to 0.034 W/(m·K) and 3906.45 J/(kg·K) to 2198.52 J/(kg·K), respectively, as the moisture content decreased from 78% to 5%. With the variable thermal and physical properties, the heat transfer simulation model made accurate predictions of the hot-air drying characteristics for the colored potatoes, and the RMSE values for all cases were (1.85±0.27)°C.

Keywords: colored potato, hot air drying, drying characteristics, computational fluid dynamics, thickness, air velocity

DOI: 10.25165/j.ijabe.20181101.3293

Citation: Park H W, Yoon W B. Effects of air movement in a hot air dryer on the drying characteristics of colored potato (*Solanum tuberosum* L.) using computational fluid dynamics. Int J Agric & Biol Eng, 2018; 11(1): 232–240.

1 Introduction

Colored potatoes are a rich source of anthocyanins or thermophilic (52°C). A pilot-scale test in a 3 m^3 household, i.e., natural pigments with antioxidative properties[1-4]. Anthocyanin level in blue- or red-fleshed potatoes is about two times higher than in regular white-fleshed potatoes[1,5,6], and the utilization of colored potatoes is highly suggested[1,7,8]. Potato products made from colored (red or purple) potatoes may be an interesting alternative to traditional products. The colored potatoes are popularly consumed as an ingredient in a salad or processed foods such as colored crisps and French fries.

Recently, powdered forms of dehydrated potatoes are in high demands in the food industry because of their convenience to apply in processed food industries[9]. Potato powders can be easily used in the processing of mashed potato, bakery products, noodles and so forth because the powders are easy to deliver and easy to mix with other food ingredients and also need less time for food preparation, compared to raw potatoes. The drying process is the most important unit operation in manufacturing potato powder. Food manufacturers commonly use a conventional hot air drying system. Air-drying causes significant changes in the vegetable and fruit structures and textures, such as softening and firmness loss[10] or surface hardening[11]. The textures of fruits and vegetables are affected by the drying processes and are strongly associated with the composition and structure of cell walls[12].

Anthocyanin, which is a natural antioxidant in colored potatoes such as purple- and red-fleshed potatoes, is easily degraded during storage and processing, particularly in heat processing[13]. Moon et al.[14] also reported that the drying temperature significantly affects the degradation of anthocyanins in colored potatoes. Several researches on the stability of the anthocyanin level and the antioxidant activity of colored potatoes during thermal processing have been reported[15-17], but very few studies have focused on the operational variables affecting dryings, such as relative humidity, velocity, and temperature of air, and material size[18-20]. In addition, these variables are very dependent on the scale or the dimensions of the dryer. Therefore, the effects of such processing variables on the drying process need to be investigated by considering dryer dimensions to achieve uniform and efficient drying. However, a simple experimental approach, 'drying-and-measure' alone may not be suitable to understand the complex interactions of these various variables.

The computational fluid dynamics (CFD) is efficiently utilized to simulate many unit operations involved in food and bioproduct processings[21-24]. Studies based on simulation models are useful for designing dryers and also for finding suitable operating conditions for existing drying systems. Many researchers reported a systematic method to predict the temperature and moisture distribution in an object containing moisture during the convective drying. Kaya et al.[25-27] developed a mass and heat transfer model for a convective drying using a cylindrical and 2-D rectangular objects. Hussain and Dincer[28] also successfully estimated the temperature and moisture content distributions in a 2-D cylindrical object. A 1-D numerical model for drying a spherical object was also developed and empirically validated[29]. Most of the reported heat and mass transfer models during the drying process simplified assumptions for simple and easy solving. In a convective drying process, significant influences are exerted

Received date: 2017-03-01 Accepted date: 2017-12-20

Biographies: Hyeon Woo Park, Graduate student, research interests: heat and mass transfer simulation, Email: hwpark0978@gmail.com.

***Corresponding author: Won Byong Yoon**, Professor, research interests: heat and mass transfer simulation. Department of Food Science and Biotechnology, College of Agricultural and Life Science, Kangwon National University, Chuncheon, Kangwondo 200-701, S. Korea. Tel: +82-33-250-6459, Fax: +82-33-241-0508, Email: wbyoon@kangwon.ac.kr.

by the drying temperature, the air flow velocity and the transfer coefficients associated with the drying temperature and air velocity. Therefore, it is needed to analyze the influences of the drying temperature and the air flow velocity in a drying chamber on the drying of colored potatoes of which characteristics are highly sensitive to the temperature.

The aims of this study are: (a) to evaluate the influences of the colored potato slices and the air temperature on drying kinetics; (b) to investigate the relationship between the flow field in the dryer and heat and mass transfer of the colored potato; and (c) to simulate heat transfer and mass transfer during the hot air drying of colored potatoes with variable property models.

2 Materials and methods

2.1 Raw materials

Purple-fleshed potatoes were donated from KIST (Korea Institute of Science and Technology) at Gangneung, S. Korea. The potatoes were carefully stored at 4°C and 80% relative humidity.

2.2 Drying process

The hot air drying experiments were carried out in a model drying system prepared by altering a commercial lab scale tray dryer (NB-901M, N-BIOTEK, Bucheon, Gyeonggi, S. Korea). The size of the chamber of the tray dryer was 550 mm × 520 mm × 600 mm. Three different sample sizes (diameter = 50 mm, thickness = 10 mm, 15 mm and 20 mm) were used to investigate the size dependence of the drying characteristics. The processing variables for the drying experiment were as follows: relative humidity (RH) of the air (10%), air velocity (3 m/s), and three levels of air temperature (50°C, 60°C and 70°C). Samples were placed at 5 different positions during the drying process (Figure 1b). The temperature in the dryer was accurately controlled within ±1°C. The RH during the drying experiment was maintained at (10±0.5)% by circulating and ventilating air in the drying chamber.

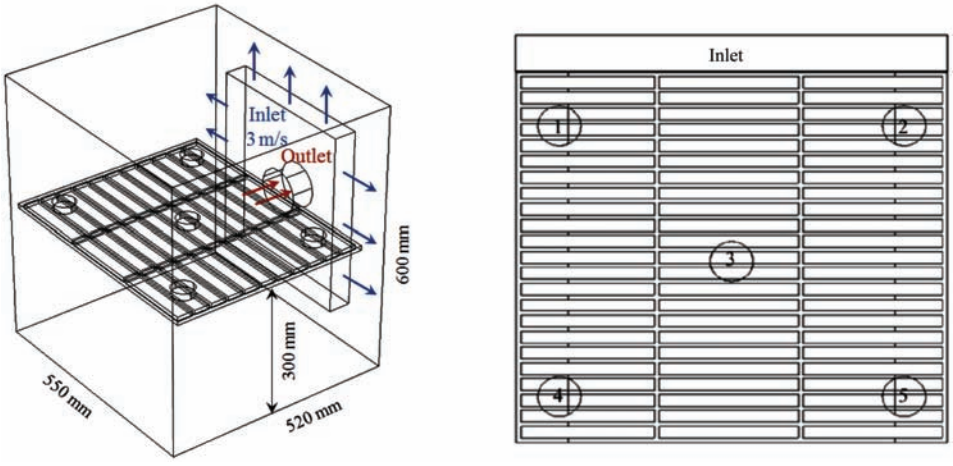

a b

Figure 1 General view of the 3-D geometrical model of the hot-air dryer and the position of sample during hot-air drying

2.3 Measuring the colored potato temperature and velocity

For the model validation, experiments were carried out to measure both the temperature and velocity during drying. Thermocouples (Vernier, Beaverton, AL, USA) were affixed to the inside body wall of the dryer to measure the chamber temperature. Additionally, a wireless temperature sensor (Tracksense® Pro, Ellab, Hilleroed, Denmark) monitored the temperature at the geometrical center of the colored potato. Temperature changes of the internal body of the colored potato during drying were measured and recorded.

2.4 Material properties

A KD2 Pro Thermal Properties Analyzer (Decagon Devices Inc., Pullman, WA, USA) was used to measure the thermal properties, such as thermal conductivity and the specific heat, of the colored potato[30]. The thermal properties were measured at 30°C, 40°C, 50°C, 60°C and 70°C over the moisture range of 5% to 78%. Ten replicate measurements were performed for each sample.

Because the density of colored potatoes is similar to those of regular potatoes, the density of a potato was determined as a function of the moisture content. The thermal and physical properties of air were determined as a function of temperature (Table 1).

Table 1 Thermal and physical properties of air, colored potato and aluminum

Property	Air	Aluminum	Potato	Colored potato
Density (ρ) /kg·m^{-3}	Ideal-gas model	2700	1.080+0.188exp(−0.433M^2)	
Thermal Conductivity (k_T) /W·(m·K)$^{-1}$	$7\cdot10^{-5}T$+0.0238	232.4		0.0281exp(0.0637M−0.00037M^2)
Specific Heat (C_p) /J·(kg·K)$^{-1}$	$6\cdot10^{-7}T^2$−$4\cdot10^{-5}T$+1	900		1776.526+6.109T+0.0269M^2
Viscosity (μ) /Pa·s	$4\cdot10^{-8}T$+$2\cdot10^{-5}$			
Thermal Expansion Coefficient (β) /K^{-1}	0.003325			
Source	[46]	COMSOL 5.1	[47]	

2.5 Numerical simulation

2.5.1 Modeling of external flow

The configuration of the dryer was measured and used for the model geometry for this study. The problem domain was schematically illustrated in Figure 1. The colored potato samples were placed inside a rectangular chamber (length: width: height = 550 mm: 520 mm: 600 mm), and hot air flows were continuously circulated in the chamber (Figure 1). The k-ε turbulence model was used to simulate the forced convection motion of the air fluid in the chamber. This model uses a specific relation to determine the local value of the eddy viscosity from the turbulent kinetic energy (k) and its dissipation (ε). The k-ε turbulence model is the

most widely used method to describe the behavior of the turbulent flow in the simulation with an assumption that the turbulence is isotropic[31-33]. This assumption is highly efficient in that the amount of time for the calculation is dramatically reduced, while the accuracy is nearly maintained. The solution domain for the CFD simulations for the flow field was set to the space in the chamber excluding the sample geometry. Thus, the interior boundaries were placed around the sample to separate it from the domain for the CFD simulation. The standard *k-ε* model employs the following turbulence transport equations[34]:

The turbulent kinetic energy equation is:

$$\frac{\partial}{\partial t}(\rho k)+\nabla\cdot(\rho\vec{v}k)=\nabla\cdot\left(\frac{\mu_t}{\sigma_k}\nabla k\right)+G_k-\rho\varepsilon \quad (1)$$

The dissipation rate equation is:

$$\frac{\partial}{\partial t}(\rho\varepsilon)+\nabla\cdot(\rho\vec{v}\varepsilon)=\nabla\cdot\left(\frac{\mu_t}{\sigma_\varepsilon}\nabla\varepsilon\right)+\frac{\varepsilon}{k}(C_1G_k-C_2\rho\varepsilon) \quad (2)$$

Combining Equations (1) and (2), the turbulent viscosity (μ_t) can be written as:

$$\mu_t=\frac{C_\mu k^2}{\varepsilon} \quad (3)$$

where, k is the turbulent kinetic energy, m^2/s^2; ρ is the density, kg/m^3, $\vec{v}$ is the velocity, m/s; G_k is the production of turbulent kinetic energy, $kg/(m\cdot s^3)$; ε is the dissipation rate, m^2/s^3, and C_μ, C_1 and C_2 are the empirical constants in the turbulence model, and σ_k and σ_ε are the turbulent Prandtl numbers for the kinetic energy and the dissipation rate, respectively. Standard values of the model constants of the *k-ε* model used in the model are referred from Pope[33]:

$$C_\mu=0.09,\ C_1=1.44,\ C_2=1.92,\ \sigma_k=1.0,\ \sigma_\varepsilon=1.3 \quad (4)$$

Simulations were carried out for the same inlet flow velocity (3 m/s). The CFD simulation was performed to calculate the heat and mass transfer coefficient around the sample placed inside the channel because the mass transfer coefficient is independent of the imposed air velocity at the inlet of the dryer.

The local mass and heat transfer coefficients are determined using the following equations adjusted for the turbulent flow around cylinder bodies, and the flow field used to estimate these coefficients was obtained from the flow filed simulation described above[35]:

$$Nu=0.683Re^{0.466}Pr^{0.333} \quad (5)$$

Equation (5) is the same as the following:

$$\frac{hL}{k}=0.683\frac{vL}{V}^{0.466}\frac{C_p\mu}{k}^{0.333} \quad (6)$$

The heat transfer coefficient is:

$$h=\left\{0.683\frac{vL}{V}^{0.466}\frac{C_p\mu}{k}^{0.333}\right\}\frac{k_T}{L} \quad (7)$$

where, *Nu* is Nusselt number; *Re* is Reynolds number; *Pr* is Prandtl number; h is the heat transfer coefficient, $W/(m^2\cdot K)$; k_T is the thermal conductivity, $W/(m\cdot K)$; L is the diameter of the cylinder, m, v is the air velocity, m/s; V is the kinematic viscosity, m^2/s; C_p is the specific heat, $J/(kg\cdot K)$ and μ is the dynamic viscosity, Pa·s.

The mass transfer coefficient was estimated based on the analogy of Fourier's law and Fick's law. Prandtl number and Nusselt number are replaced by Schmidt number and Sherwood number, respectively, giving the following relationship[35]:

$$Sh=0.683Re^{0.466}Sc^{0.333} \quad (8)$$

Equation (8) is the same as following:

$$\frac{h_mL}{D}=0.683\frac{vL}{V}^{0.466}\frac{V}{D}^{0.333} \quad (9)$$

The mass transfer coefficient is:

$$h_m=\left\{0.683\frac{vL}{V}^{0.466}\frac{V}{D}^{0.333}\right\}\frac{D_m}{L} \quad (10)$$

where, *Sh* is Sherwood number; *Sc* is Schmidt number; h_m is the mass transfer coefficient, m/s and D is the mass diffusivity, m^2/s.

In the equations above, all properties are evaluated at a mean boundary layer temperature (T_f), also called the film temperature. The film temperature is given by:

$$T_f=\frac{T_\infty+T_s}{2} \quad (11)$$

where, T_∞ is the air temperature, °C; T_s is the temperature on the surface of sample, °C.

2.5.2 Modeling of the internal temperature and moisture fields of the sample

A mathematical model is developed to interpret the mass and heat transfer occurring in the samples being dried. The shrinkage and deformation of the sample, the internal heat generation, and the radiation effect were ignored in the simulation. Under the assumptions above, the governing heat and mass transfer equations can be written as[36]:

$$\frac{1}{\alpha}\frac{\partial T}{\partial t}=\frac{\partial^2T}{\partial z^2}+\frac{\partial^2T}{\partial r^2} \quad (12)$$

$$\frac{1}{D}\frac{\partial M}{\partial t}=\frac{\partial^2M}{\partial z^2}+\frac{\partial^2M}{\partial r^2} \quad (13)$$

The initial conditions are:

$$T(z,r,0)=T_i \text{ and } M(z,r,0)=M_i \quad (14)$$

The boundary conditions are:

$$z=0,\ \frac{\partial T}{\partial z}=0 \text{ and } \frac{\partial M}{\partial z}=0 \quad (15)$$

$$r=0,\ \frac{\partial T}{\partial r}=0 \text{ and } \frac{\partial M}{\partial r}=0 \quad (16)$$

and on the surface:

$$k_T\frac{\partial M}{\partial z}=h(T_\infty-T_s) \text{ and } k_T\frac{\partial T}{\partial r}=h(T_\infty-T_s) \quad (17)$$

$$D\frac{\partial M}{\partial z}=h_m(M_\infty-M_s) \text{ and } D\frac{\partial M}{\partial r}=h_m(M_\infty-M_s) \quad (18)$$

where, α is the thermal diffusivity; T_i is the initial temperature and M_i is the initial moisture content. The moisture diffusivity in this study were determined from the highly-referenced work of Moon et al.[12] The experimental study of Moon et al.[12] focused on the convective drying of purple-fleshed potato with 50 mm of diameter and 10 mm of thickness to study the effects of the drying temperature on the moisture diffusivity. The initial temperature of the sample was 15°C measured experimentally, and the heating medium temperatures were controlled to 50°C, 60°C and 70°C. A no-slip condition was applied on the outer boundaries to solve the momentum equations.

2.6 Simulation

A commercial finite element analysis software, COMSOL Multiphysics 5.1 program (COMSOL Multiphysics, Stockholm, Sweden), was utilized to simulate the drying process. Density, specific heat, and thermal conductivity are taken as variable properties depending on the moisture content and temperature while solving the heat and mass transfer equations. Local mass and heat transfer coefficients of each sample are also taken as variable properties with respect to the flow field around the sample.

The mass and heat transfer equations are coupled and solved simultaneously. Simulations were carried out with an Intel® Core™ i7-3770 3.4 GHz PC with 16 Gigabytes of RAM running Windows 7 64-bit edition.

2.7 Evaluation of the validity of the simulation results

The results of the simulation for the transient temperature and moisture content during drying were evaluated by comparing to the experimental data. In general, the validity of the model is assessed by the root mean square error (RMSE)[37-39].

The *RMSE* is given by:

for moisture content,

$$RMSE = \sqrt{\frac{1}{N} \cdot \sum_{i=1}^{N} (MR - MR_{simulation})^2} \quad (19a)$$

for temperature,

$$RMSE = \sqrt{\frac{1}{N} \cdot \sum_{i=1}^{N} (T - T_{simulation})^2} \quad (19b)$$

where, MR is the moisture ratio (M/M_i). The temperatures experimentally measured at the geometrical center during thermal treatment along with those obtained from the simulation were used to calculate the *RMSE*.

3 Results and discussion

3.1 Flow fields of hot air in the dryer

The flow fields of hot air in the dryer were simulated using CFD. The velocity vectors are illustrated in Figure 2. Flow fields, which influenced the drying efficiency of the hot air dryer, were highly dependent on the layout of the dryer. The local air velocity was estimated at each sample position (Table 2). It slightly deviated from the symmetricity. Generally, the exact analytical solutions for the turbulent boundary layer is not provided, which was inherently unsteady[35].

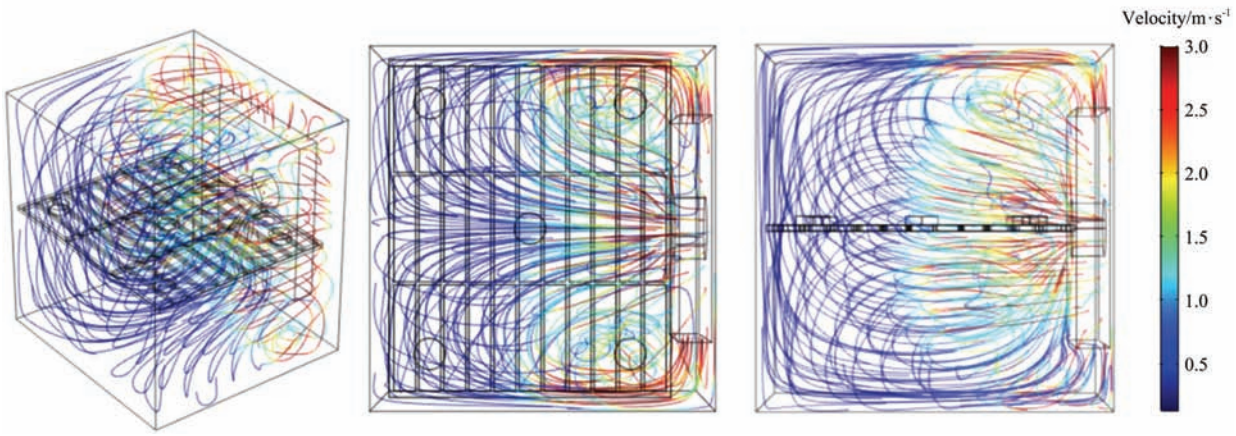

Figure 2 Velocity vector field in the 3-D hot-air dryer domain at 60°C.

Table 2 Effect of the position in the tray dryer on the air velocity and heat and mass transfer coefficients

	Position				
	1	2	3	4	5
Air velocity/m·s^{-1}	1.560	1.573	0.753	0.208	0.206
Heat transfer coefficient/W·(m^2·K)$^{-1}$	16.83		11.97		6.555
Mass transfer coefficient/10^{-3} m·s^{-1}	14.82 + 0.04710T_f		10.15 + 0.03348T_f		5.562 + 0.01834T_f

Even though the estimated local air velocity slightly deviated from symmetricity, this variation could be neglected due to the variation at a different position being much higher. The local heat and mass transfer coefficients were estimated at different positions of the sample (Table 2). The effect of the film temperature on the heat transfer coefficient was relatively minor within the range of temperature studied (<0.0403 W/m^2·K) while the mass transfer coefficient increased linearly as the film temperature increased. The average air velocity was evaluated from the two symmetrical points such as 1 and 2, and 4 and 5 described in Figure 1. The highest velocity was observed at position 1 and 2 where the flow inlet is nearly located. The local air velocity decreased as the distance from the inlet flows increased. The maximum heat and mass transfer coefficients at 60°C film temperature were obtained at position 1 and were 16.83 W/(m^2·K) and 0.01755 m/s, respectively. These values were much higher than the heat and mass transfer coefficients at position 5, which were 6.555 W/(m^2·K) and 0.006835 m/s. Because the different heat and mass transfer coefficient distributions by the flow field within a dryer may cause a non-uniform drying quality, the effect of air velocity in accordance with the position on the heat and mass transfer during hot air drying must be examined for drying colored potatoes.

3.2 Drying characteristics of the colored potato and validation of the simulation model

The effect of the local air velocity on the drying of the colored potato at different positions was shown in Figure 3. As expected, the air velocity significantly affected the drying rate of the colored potato during the hot air drying. Usually, it is known that an increase in the air velocity results in a decreasing moisture ratio at each axial position due to increasing convective heat and mass transfer between the hot air and food. According to Aghbashlo et al.[40], the higher drying air temperature and air velocity caused an increase of drying rate because of a higher rate of mass transfer. Vega-Gálvez et al.[41] reported that increasing the air velocity increased the drying rate of an apple slice because of a higher rate of heat and mass transfer. These results clearly demonstrated that a faster air velocity leads to faster drying.

The simulation using the mass transfer model was validated with experiment data (Figures 3 and 4). The validity of the mass transfer model was estimated by comparing the simulation results with the experimental results at different air flows and thickness, and the RMSE values for all cases were less than 0.057. Generally,

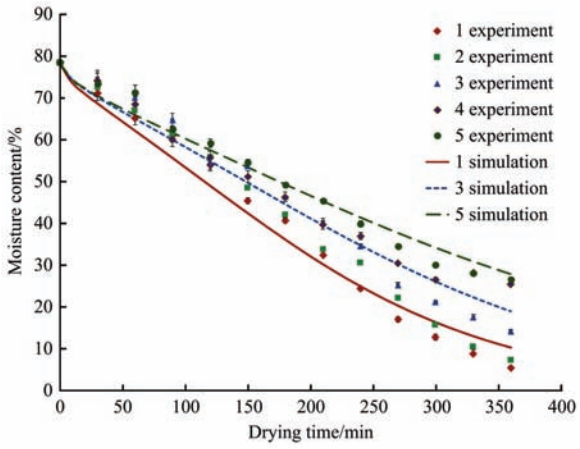

a. 50°C

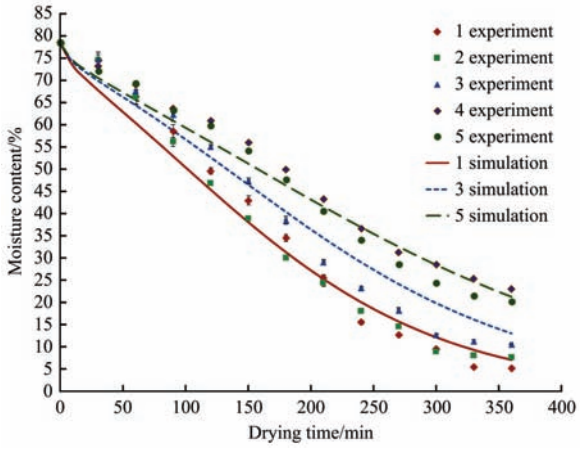

b. 60°C

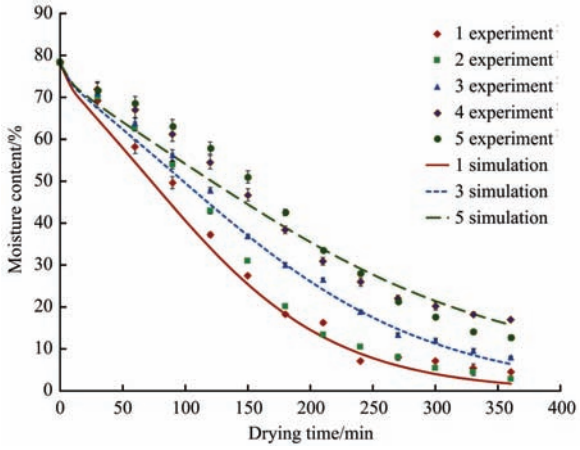

c. 70°C

Figure 3 Comparison of mass transfer simulation results with the experimental data of the colored potato with 10 mm of thickness during hot-air drying at different positions in the dryer

RMSE value of less than 0.060 was used to validate the prediction model of drying process[42,43]. The results indicated that the moisture content predicted from the model closely agreed with the moisture content measured experimentally. The model developed in this study can predict the drying times at different flow fields and temperatures. The stability during conservation is highly dependent on the residual moisture content of the final product. Figure 5 shows the moisture distribution predicted at different positions in the dryer and temperatures. As expected, the differences in the moisture distribution caused by the effect of the flow field in the hot-air dryer increased as the drying time and temperature increased. Therefore, this study suggested that the moisture content for a stable preservation should be estimated based on the local moisture content rather than on the average moisture content. If there is a moisture gradient in the products being dried, the moisture content at certain points may exceed the critical moisture content which guarantees a stable preservation during storage and distribution. As a result, microbiological deterioration might take place in a specific portion of the product before reaching the equilibrium moisture content. The simulation results from this study clearly demonstrated that local moisture content could be estimated based on the mass and heat transfer models, and it provides useful information to control the shelf life of the dried products.

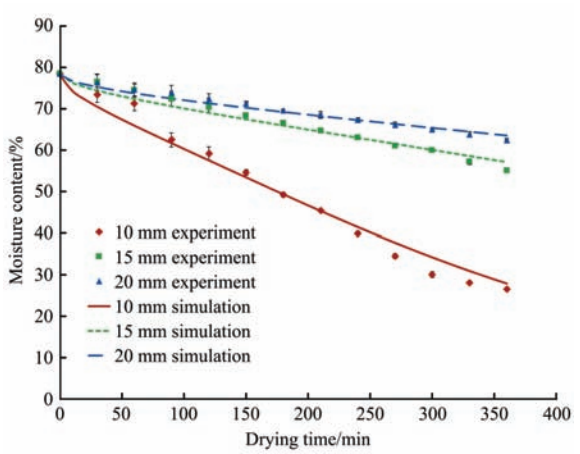

a. 50°C

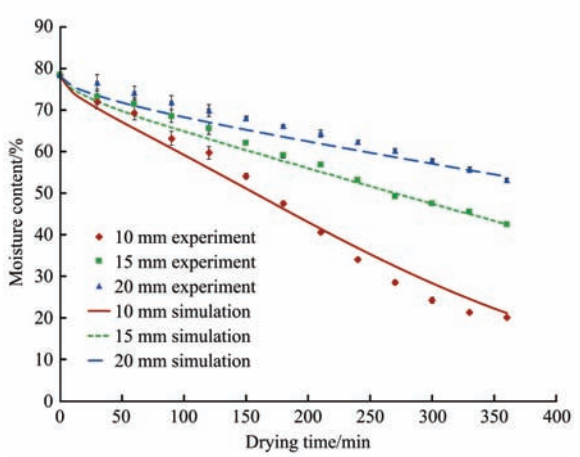

b. 60°C

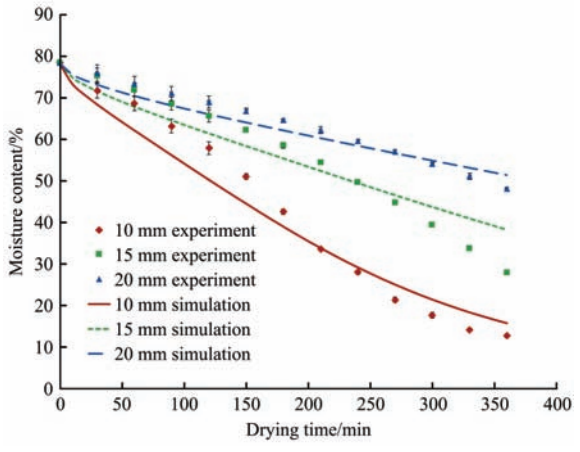

c. 70°C

Figure 4 Comparison of mass transfer simulation results with the experimental data of the colored potato during hot-air drying at position 5 in the dryer

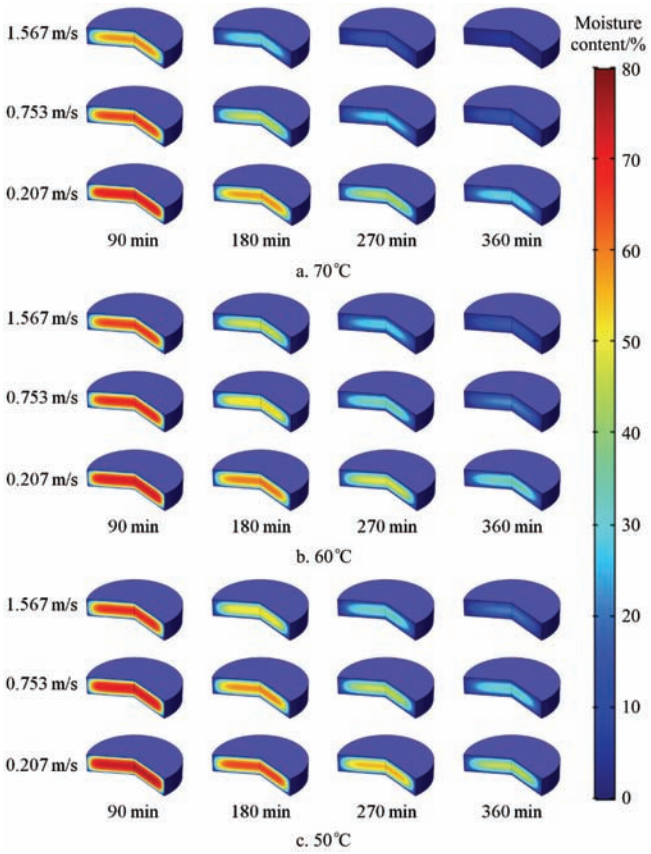

Figure 5 Moisture distribution of the colored potato at different positions in the dryer during hot-air drying at 70°C, 60°C and 50°C

3.3 Heat transfer characteristics of the colored potato and validation of the simulation model

The specific heat of the colored potato with the moisture content range of 5 to 78% was measured at 30°C, 40°C, 50°C, 60°C and 70°C. Because the specific heat of a solid is highly dependent on the temperature, increasing the moisture content significantly affected the specific heat of the colored potato (p<0.05)[44]. A higher specific heat is found in food with higher moisture contents[45-47]. Wang and Brennan[48] reported that the specific heat of a potato was between 0.4 cal/(g·°C) and 0.9 cal/(g·°C), which was similar to the specific heat of the colored potato measured in this study. A model for the specific heat of the colored potato as a function of temperature (T) and moisture content (M) was developed by fitting the experimentally measured values (R^2 = 0.99) (Table 1).

Thermal conductivity increased with increasing moisture content from 5% to 78%±0.2% while it was not significantly influenced by the temperature (30°C, 40°C, 50°C, 60°C and 70°C). The thermal conductivity increased from 0.034 W/(m·K) to 0.440 W/(m·K) as the moisture content increased from 5% to 78%. The increased thermal conductivity with increasing moisture content was because of the high thermal conductivity of water compared to that of other components in the colored potato. Similarly, the thermal conductivity of the potato (0-5 kg/kg d.b.) ranged from 0.03 W/(m·K) to 0.46 W/(m·K) over the temperature range of 40°C to 70°C[49]. A model was developed for the thermal conductivity of the colored potato as a function of the moisture content with an R^2 of 0.99 (Table 1). Our study demonstrated that the thermal conductivity of colored potatoes changed significantly regarding the moisture content.

The temperature distribution of the colored potatoes during the drying process needs to be predicted accurately because the anthocyanins in colored potatoes are easily degraded during thermal treatment. During the drying process, thermal and physical properties such as thermal conductivity, specific heat, and density are highly dependent on the moisture content. Therefore, to predict the temperature distribution of the colored potato during the drying process, thermal and physical properties should be considered as variable functions when the drying process of the colored potato is simulated. The simulation of the drying process was implemented in the COMSOL Multiphysics 5.1 program to predict the transient temperature profiles of samples at different air temperatures of 50°C, 60°C and 70°C. Thermal conductivity,

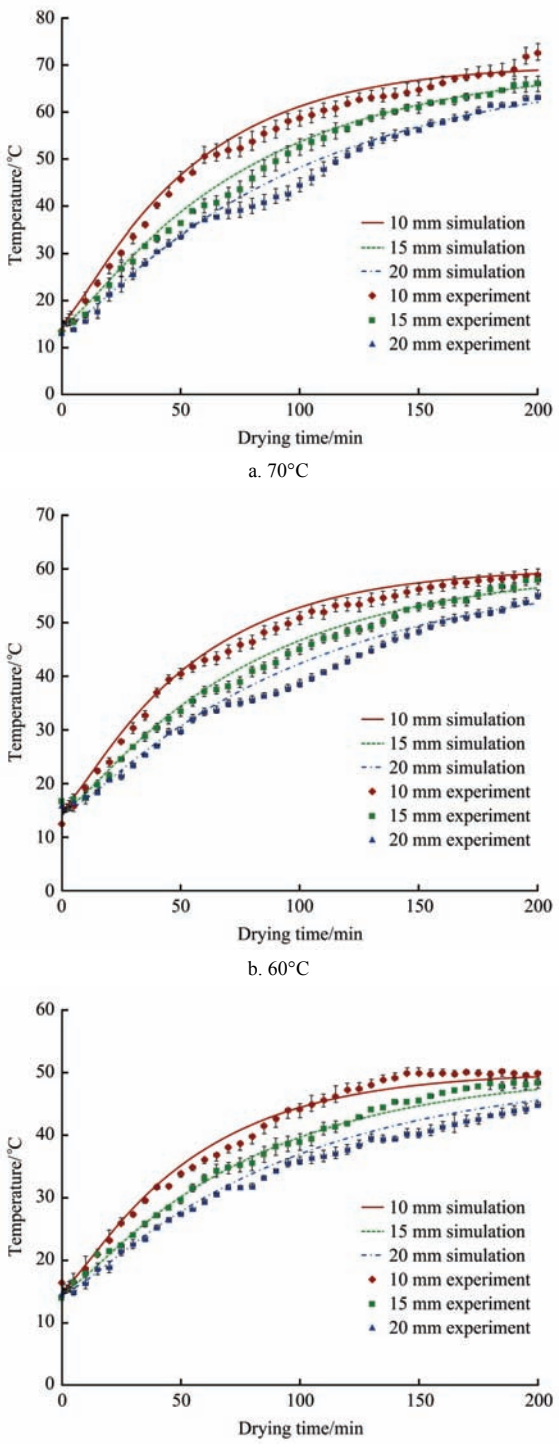

Figure 6 Comparison of heat transfer simulation results with the experimental data of the colored potato during hot-air drying at position 3 in the dryer

specific heat, and density were taken as variable properties depending on the temperature and the moisture content of the samples while solving the heat and mass transfer equations. Local heat and mass transfer coefficients of each sample are also taken as variable properties with respect to the flow field at the sample position. The heat and mass transfer equations are solved simultaneously. The model was validated by comparing the temperatures with the experimental results (Figure 6). The RMSE values calculated using Equation (19) for all cases were (1.85± 0.27)°C. In general, RMSE value for the heat transfer simulation model should be less than 5°C[37-39]. The results demonstrated that the simulation model suitably described the temperature profiles in the dryer with variable thermal and physical properties.

With constant values of thermal properties, such as k and C_p, the temperature distribution in the colored potato was simulated and plotted every 50 min during drying at 70°C (Figure 7). The constant values of the thermal properties were calculated with the initial moisture content of the colored potato (78.45%). The thermal conductivity of the colored potato was highly dependent on the moisture content rather than the temperature within the range studied (30°C-70°C). In the constant k model, there were no significant temperature gradients because of the thermal conductivity, which was high enough for constantly conducting heat from the surface to the inside. This was in contrast with the variable model result in that the local thermal conductivity decreased from 0.4270 W/(m·K) to nearly 0 W/(m·K) at the surface of the colored potato. In the variable model, the local C_p at the surface decreased rapidly as the moisture content at the surface decreased. The decreased C_p easily increased the surface temperature, producing a temperature gradient for heat transfer, which was in contrast to the results of the constant C_p model in that the local C_p at the surface was the same as that on the inside.

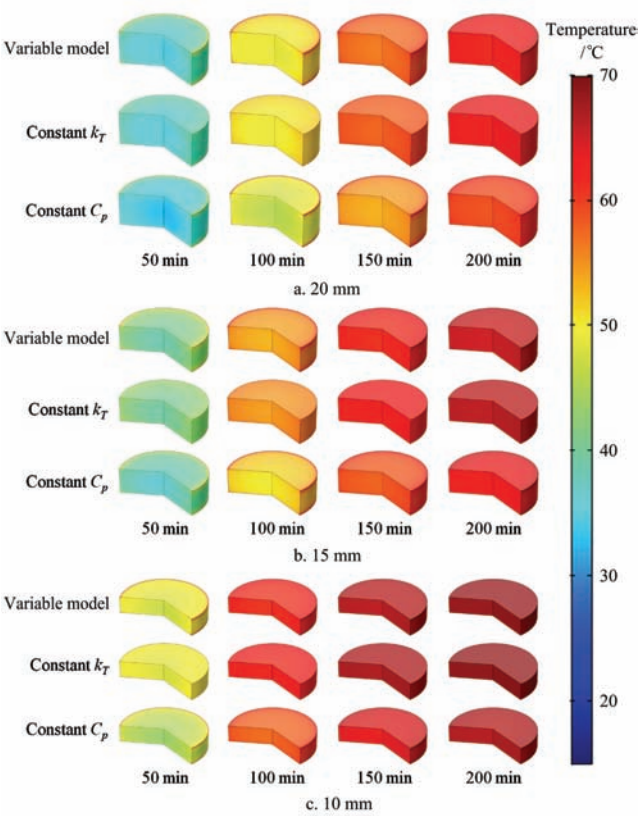

Figure 7 Temperature distribution of the colored potato with thicknesses of 20 mm, 15 mm and 10 mm during hot-air drying at 70°C.

Obviously, the temperature distribution difference increased as the thickness of the sample decreased because the drying rate of the colored potato increased as the sample thickness increased. It should be noted here that the constant k_T and C_p models showed significant differences with the variable model. This result clearly demonstrated that the thermal properties during hot-air drying should be considered as variables for the heat transfer model, especially in the simulation of a material that has a high moisture content and is easily susceptible to deterioration through temperature.

4 Conclusions

The flow fields of the hot air in the dryer were simulated using CFD. The local air velocity decreased as the distance from the flow inlet and outlet increased, which is in the range of 0.207 m/s to 1.566 m/s. Since the different heat and mass transfer coefficient distribution by the flow field within a dryer may cause a non-uniform drying quality, the effect of air velocity at the different positions on the heat and mass transfer during hot air drying must be examined for colored potatoes because of the high heat sensitivity of anthocyanins. The drying simulation model using heat and mass transfer models accurately predicted the drying characteristics of colored potatoes in the hot-air drying system. Thermal properties of colored potato, such as specific heat and thermal conductivity significantly decreased from 3906.45 J/(kg·K) to 2198.52 J/(kg·K) and from 0.440 W/(m·K) to 0.034 W/(m·K) as the moisture content decreased 78% to 5%, respectively. The temperature and the moisture distribution in the colored potato samples were successfully predicted by the step-by-step simulation suggested from this study. The flow filed was simulated in the first step, then the heat and mass transfer coefficients were estimated based on the flow filed simulation results. Finally, the moisture and the temperature distribution was predicted by solving the governing partial differential equations using CFD. The model verification was performed by comparing the simulation results with the experimental results, and the RMSE values for all cases were less than (1.85±0.27)°C. Therefore, the simulation model was successfully developed with the variable thermal and physical properties to predict the moisture and temperature changes of colored potato during drying. The simulation model in this study can provide useful information to control the quality of the colored potato products, such as moisture content and anthocyanin, during drying by predicting moisture and temperature distribution of the products.

Acknowledgements

This work was supported by Korea Institute of Planning and Evaluation for Technology in Food, Agriculture, Forestry and Fisheries (IPET) thorugh High Value-added Food Technology Development Program, funded by Minstry of Agriculture, Food and Rural Affairs (Grant No. 314047-2). This study has been worked with the support of a research grant of Kangwon National University in 2016.

Nomenclature

C_p	Specific heat (J/(kg·K))
D	Moisture diffusivity (m^2/s)
h	Heat transfer coefficient (W/(m^2·K))
h_m	Mass transfer coefficient (m/s)

k	Turbulent kinetic energy (m^2/s^2)
k_T	Thermal conductivity (W/(m·K))
L	Diameter of cylinder (m)
M	Moisture content (g/g d.b.)
T	Temperature (°C)
T_f	Film temperature (°C)
v	Air velocity (m/s)
V	Kinematic viscosity (m^2/s)
Greek symbols	
α	Thermal diffusivity (m^2/s)
ρ	Density (kg/m^3)
μ	Dynamic viscosity (Pa·s)
ε	Dissipation rate (m^2/s^3)
Subscripts	
i	Initial condition
∞	Air condition

[References]

[1] Lachman J, Hamouz K. Red and purple colored potatoes as a significant antioxidant source in human nutrition – A review. Plant Soil and Environment, 2005; 51(11): 477–482.

[2] Lachman J, Hamouz K, Šulc M, Orsák M, Pivec V, Hejtmánková A, et al. Cultivar differences of total anthocyanins and anthocyanidins in red and purple-fleshed potatoes and their relation to antioxidant activity. Food Chemistry, 2009; 114: 836–843.

[3] Rodrigez-Saona L E, Giusti M M, Wrolstad R E. Anthocyanin pigment composition of red-fleshed potatoes. Journal of Food Science, 1998; 63: 458–465.

[4] Wegener C B, Jansen G. Soft-rot resistance of coloured potato cultivars (*Solanum tuberosum* L.): the role of anthocyanins. Potato Research, 2007; 50(1): 31–44.

[5] Brown C R, Wrolstad R, Durst R, Yang C P, Clevidence B. Breeding studies in potatoes containing high concentrations of anthocyanins. American Journal of Potato Research, 2003; 80: 241–250.

[6] Hejtmánková K, Pivec V, Trnkova E, Hamouz K, Lachamn J. Quality of coloured varieties of potatoes. Czech Journal of Food Science, 2009; 27: S310–S313.

[7] Friedman M. Potato glycoalkaloids and metabolites: Role in the plant and in the diet. Journal of Agricultural and Food Chemistry, 2006; 54: 8655–8681.

[8] Friedman M, McDonald G. Potato glycoalkaloids: Chemistry, analysis, safety and plant physiology. Critical Reviews in Plant Science, 1997; 16(1): 55–132.

[9] Carillo P, Cacace D, de Rosa M, de Martino E, Cozzolino C, Nacca F, et al. Process optimisation and physicochemical characterisation of potato powder. International Journal of Food Science & Technology, 2009; 44(1): 145–151.

[10] Ramos I N, Silva C L M, Sereno A M, Aguilera J M. Quantification of microstructural changes during first stage air drying of grape tissue. Journal of Food Engineering, 2004; 62: 159–164.

[11] Orikasa T, Tagawa A, Soma S, Iimoto M, Ogawa Y. Hot air drying characteristics of fruits and vegetables and surface hardening of samples during drying. Journal of the Japanese Society of Agricultural Machinery, 2005; 67(6): 62–70.

[12] Ramos I N, Brandão T R S, Silva C L M. Structural changes during air drying of fruits and vegetables. Food Science Technology International, 2003; 9(3): 201–206.

[13] Reyes L F, Cisneros-Zevallos L. Degradation kinetics and color of anthocyanin in aqueous extracts of purple- and red-flesh potatoes (*Solanum tuberosum* L.). Food Chemistry, 2007; 100: 885–894.

[14] Moon J H, Pan C H, Yoon W B. Drying characteristics and thermal degradation kinetics of hardness, anthocyanin content and colour in purple - and red - fleshed potato (*Solanum tuberosum* L.) during hot air drying. International Journal of Food Science & Technology, 2015; 50(5): 1255–1267.

[15] Kita A, Bakowska-Barczak A, Hamouz K, Kuakowska K, Lisińska G. The effect of frying on anthocyanin stability and antioxidant activity of crisps form red- and purple-fleshed potatoes (*Solanum tuberosum* L.). Journal of Food Composition and Analysis, 2013; 32: 169–175.

[16] Lachman J, Hamouz K, Orsák M, Pivec V, Hejtmánková K, Pazderů K, et al. Impact of selected factors-cultivar, storage, cooking and baking on the content of anthocyanins in coloured-flesh potatoes. Food Chemistry, 2012; 133: 1107–1116.

[17] Nayak B, Berrios J, Powers J R, Tang J, Ji Y. Colored potatoes (*Solanum tuberosum* L.) dried for antioxidant-rich valued added foods. Journal of Food Processing and Preservation, 2011; 35: 571–580.

[18] Karathanos V T, Belessiotis V G. Sun and artificial air drying kinetics of some agricultural products. Journal of Food Engineering, 1997; 31(1): 35–46.

[19] Lee S K, Voung R E, Schiffman P M, Coggins C W. Maturity studies of arocade fruit based on picking dates and dry weight. Journal of the American Society of Agricultural Science, 1983; 180: 390–394.

[20] Mulet A, Berna A, Rossello C. Drying of carrots. I. drying models. Drying Technology, 1989; 7(3): 537–557.

[21] Mirade P S. Computational fluid dynamics (CFD) modelling applied to the ripening of fermented food products: Basics and advances. Trends in Food Science & Technology, 2008; 19: 472–481.

[22] Smale N J, Moureh J, Cortella G. A review of numerical models of airflow in refrigerated food applications. International Journal of Refrigeration, 2006; 29: 911–930.

[23] Wang L, Sun D W. Recent developments in numerical modelling of heating and cooling processes in the food industry–A review. Trends in Food Science and Technology, 2003; 14: 408–423.

[24] Xia B, Sun D W. Applications of computational fluid dynamics (CFD) in the food industry: a review. Computers and Electronics in Agriculture, 2002; 34(1): 5–24.

[25] Kaya A, Aydın O, Dincer I. Numerical modeling of heat and mass transfer during forced convection drying of rectangular moist objects. International Journal of Heat and Mass Transfer, 2006; 49: 3094–3103.

[26] Kaya A, Aydın O, Dincer I. Heat and mass transfer modeling of recirculating flows during air drying of moist objects for various dryer configurations. Numerical Heat Transfer, Part A: Applications, 2007; 53(1): 18–34.

[27] Kaya A, Aydın O, Dincer I. Numerical modeling of forced convection drying of cylindrical moist objects. Numerical Heat Transfer, Part A: Applications, 2007; 51(9): 843–854.

[28] Hussain M M, Dincer I. Two-dimensional heat and moisture transfer analysis of a cylindrical moist object subjected to drying: a finite-difference approach. International Journal of Heat and Mass Transfer, 2003; 46: 4033–4039.

[29] Datta A K, Teixeira A A. Numerically predicted transient temperature and velocity profiles during natural convection heating of canned liquid foods. Journal of Food Science, 1988; 53(1): 191–195.

[30] Mahapatra A K, Melton S L, Isang E M. Effect of moisture content on thermal properties. Agricultural Engineering International: CIGR Journal, 2013; 15(2): 251–255.

[31] Lam C K G, Bremhorst K A. Modified form of k-ε model for predicting wall turbulence. Journal of Fluids Engineering, 1981; 103(3): 456–460.

[32] Menter F R. Two-equation eddy-viscosity turbulence models for engineering applications. AIAA Journal, 1994; 32(8): 1598–1605.

[33] Pope S B. Turbulent Flows. Cambridge: Cambridge University Press, 2000.

[34] Wilcox D C. Turbulence modeling for CFD (Vol. 2). La Canada: DCW industries, 1988.

[35] Bergman T L, Incropera F P, Lavine A S. Fundamentals of heat and mass transfer. New Jersey: John Wiley & Sons, 2011.

[36] Mohan V P C, Talukdar P. Three dimensional numerical modeling of simultaneous heat and moisture transfer in a moist object subjected to convective drying. International Journal of Heat and Mass Transfer, 2010; 53(21-22): 4638–4650.

[37] Hong Y K, Uhm J, Yoon W B. Using numerical analysis to develop and evaluate the method of high temperature Sous-Vide to soften carrot texture in different-sized packages. Journal of Food Science, 2014; 79(4): E546–E561.

[38] Lee M G, Yoon W B. Developing an effective method to determine the deviation of F value upon the location of a still can during convection heating using CFD and subzones. Journal of Food Process Engineering, 2014; 37(5): 493–505.

[39] Lee M G, Yoon W B. Developing an effective method to determine the heat transfer model in fish myofibrillar protein paste with computer simulation considering the phase transition on various dimensions. International Journal of Food Engineering, 2016; 12(9): 889–900.
[40] Aghbashlo M, Kianmehr M H, Arabhosseini A. Modeling of thin-layer drying of potato slices in length of continuous band dryer. Energy Conversion and Management, 2009; 50(5): 1348–1355.
[41] Vega-Gálvez A, Ah-Hen K, Chacana M, Vergara J, Martínez-Monzóc J, García-Segoviac P, Lemus-Mondaca R, Scala K D. Effect of temperature and air velocity on drying kinetics antioxidant capacity, total phenolic content, colour, texture and microstructure of apple (var. *Granny Smith*) slices. Food Chemistry, 2012; 132(1): 51–59.
[42] Akpinar E K. Mathematical modelling of thin layer drying process under open sun of some aromatic plants. Journal of Food Engineering, 2006; 77(4): 864–870.
[43] Doymaz I. The kinetics of forced convective air-drying of pumpkin slices. Journal of Food Engineering, 2007; 79(1): 243–248.
[44] Engel T, Reid P. Thermodynamics, statistical thermodynamics, & kinetics (3th ed.). Washington: University of Washington 2012.
[45] Noel T R, Ring S G. A study of the heat capacity of starch/water mixtures. Carbohydrate Research, 1992; 227: 203–213.
[46] Sopade P A, LeGrys G A. Specific heat capacity of starch-sucrose systems. Food Control, 1991; 2(1): 50–52.
[47] Taiwo K A, Akanbi C T, Ajibola O O. Thermal properties of ground and hydrated cowpea. Journal of Food Engineering, 1996; 29(3): 249–256.
[48] Wang N, Brennan J G. The influence of moisture content and temperature on the specific heat of potato measured by differential scanning calorimetry. Journal of Food Engineering, 1993; 19(3): 303–310.
[49] Wang N, Brennan J G. Thermal conductivity of potato as a function of moisture content. Journal of Food Engineering, 1992; 17: 153–160.
[50] Smolka J, Nowak A J, Rybarz D. Improved 3-D temperature uniformity in a laboratory drying oven based on experimentally validated CFD computation. Journal of Food Engineering, 2010; 97: 373–383.
[51] Wang N, Brennan J G. Changes in structure, density and porosity of potato during dehydration. Journal of Food Engineering, 1995; 24(1): 61–76.